Review of Scientific Instruments ARTICLE scitation.org/journal/rsi

Ion temperature measurements from tomographic reconstruction of Doppler spectra in the presence of multi-component flow in two dimensions

Cite as: Rev. Sci. Instrum. 92, 063508 (2021); doi: 10.1063/5.0043808
Submitted: 11 January 2021 • Accepted: 17 May 2021 •
Published Online: 7 June 2021

A. Goodman,[a),b)] J. Yoo, J. Jara-Almonte, and H. Ji

AFFILIATIONS

Princeton Plasma Physics Laboratory, 100 Stellarator Rd., Princeton, New Jersey 08540, USA

Note: Paper published as part of the Special Topic on Proceedings of the 23rd Topical Conference on High-Temperature Plasma Diagnostics.
[a)]**Author to whom correspondence should be addressed:** aagoodma@pppl.gov
[b)]**Present Address:** Department of Mechanical and Aerospace Engineering, Princeton University, Princeton, New Jersey 08540, USA.

ABSTRACT

A new ion Doppler diagnostic has been constructed to measure ion temperature profiles in the presence of multi-component flow during magnetic reconnection experiments. The inversion technique and diagnostic setup are applicable to axisymmetric plasmas with two-component flow across the measurement cross section, which occurs during magnetic reconnection. The particular design discussed here is optimized for operation on the Magnetic Reconnection eXperiment (MRX) at Princeton Plasma Physics Laboratory. To prove the viability of this diagnostic for MRX and the future Facility for Laboratory Reconnection Experiments, measurements have been taken and ion temperature and perpendicular flow profiles have been obtained. The radial velocity on MRX does not contribute to the Doppler shift of the measured spectra but does contribute to the broadening of the spectra, while toroidal flow contributes to both. It is shown that neglecting the radial velocity for $v_R = 20$ km/s leads to an error in the ion temperature inversion of 20%. Results from MRX discharges are shown, and the impact of radial velocity on ion temperature inversions is discussed.

I. INTRODUCTION

The ion temperature and flow are of paramount importance in understanding energy conversion during magnetic reconnection.[1] Previous work suggests that roughly two-thirds of the converted magnetic energy is transferred to ions during a typical anti-parallel magnetic reconnection event.[2] To study the energization of ions during reconnection, it is necessary to simultaneously measure changes in thermal energy and flow velocity of ions. Previously, ion temperature measurements on the Magnetic Reconnection eXperiment (MRX)[3] were made with an Ion Doppler Spectroscopy Probe,[4] which makes a line integrated measurement for a single chord in a local volume for each discharge. Constructing a two-dimensional profile required hundreds of nearly identical discharges. Velocity measurements are made using Mach probes that have ~15% error for typical flow during MRX operation and perturb plasma around the measurement site.[5]

The spectroscopy system discussed here is capable of reconstructing full radial profiles of emissivity, toroidal velocity, and ion temperature for each discharge on MRX and the Facility for Laboratory Reconnection Experiments (FLARE).[6] The new diagnostic presented here draws on previous work using Abel and Radon transforms in plasma diagnostics.[7–9] Radial flow, which necessarily exists in reconnection experiments as reconnection inflow, can contribute significantly to the Doppler broadening of measured spectra and complicate the application of tomographic methods. Previous diagnostics on reconnection experiments have not properly accounted for the broadening of spectra due to radial velocity when inverting the ion temperature.[10] This is the first implementation, to the authors' knowledge, of a tomographic system on a

reconnection experiment that properly handles the broadening due to radial velocity in temperature inversions.

The rest of this paper is structured as follows: the experimental setup and hardware are outlined in Sec. II and the theory behind the tomographic inversion and the effect of radial flow is discussed in Sec. III. Initial results from an MRX experiment employing this new diagnostic are presented in Sec. V, and the inversion method used in the experiment is tested in Sec. IV.

II. EMISSION MEASUREMENT SYSTEM

MRX is a cylindrical vacuum vessel with four sets of coils that produce plasma and the magnetic configuration necessary for reconnection studies. The MRX coordinate system and geometry are shown in Fig. 1(a). Figure 1(b) shows the geometry of the measurement plane, and Fig. 1(c) shows the calibration lamp and the path of light through fiber optics (red) to the spectrometer. In this paper, "in-plane" refers to the $R - Z$ plane, out-of-plane, the perpendicular direction, or "toroidal" refers to the ϕ direction, and measurement cross sections refer to the $R - \phi$ plane.

This measurement system is built for an axisymmetric plasma configuration and covers 37.5° or equivalently a radial extent of 16.6 cm when measured at the tangency radii. It is designed to resolve ion temperatures of at least 10 eV and toroidal velocities of ≤ 8 km/s in ≈ 1 cm increments, with gate times of $\leq 20\ \mu$s. The radius of the MRX vacuum vessel is 76.2 cm. The edge of the plasma is poorly defined, and although emission drops to undetectable levels beyond $R = 44$ cm in most of the data collected, the lack of a plasma edge can lead to errors on the low radius side of the inversion. For this experiment, the measurement region spans from $R = 28.6$ cm to $R = 45.2$ cm. Light was collected through the view port on the bottom of the MRX device. A helium calibration lamp was used to correct for shot-by-shot variation in the detector position caused by vibrations associated with MRX discharges.

This experiment has 16, 400 μm core diameter fibers with an outer cladding diameter of 560 μm and a numerical aperture of 0.22 for light collection. These fibers are arranged linearly on the face of a cylindrical ferrule at a depth of 46.5 mm behind a 50 mm focal length camera lens (NIKKOR Model No. FBA_2137) focused at infinity. The separation of the fibers is 760 μm center-to-center. The spatial resolution measuring the distance between tangency radii of the viewing chords is ~1 cm. The spot size at the tangency radius is ~0.8 cm. One additional fiber, not placed behind the collection lens, is focused on a helium calibration lamp to correct for shot-by-shot variation of the detector position and is shown schematically in Fig. 1(c). The fibers carry plasma emission to a Czerny–Turner type, f/7 McPherson spectrometer (Model No. 2061, 1 m focal length and a grating frequency of 2400lines mm^{-1}) connected to a PI-MAX2 Intensified Charged Coupled Device (ICCD) detector (1024 × 1024 pixel grid with 13.1 μm pixel width and a quantum efficiency of ~47%). The dispersion of the instrument was $0.003\,98 \pm 6.9 \times 10^{-6}$ nm/pixel for this experiment. The etendue of the system is 1.533e − 4mm^{2}sr. This setup has a temporal resolution controlled by the gate time of the ICCD. For this experiment, shot 185 006 (Figs. 2 and 5), as well as most other shots collected in the campaign, is temporally resolved to 10 μs.

Figure 2(a) shows raw data from the detector for discharge 185 006. Figure 2(b) shows the spectra for channels (corresponding to tangency radii) 4 (31.15 cm), 6 (33.78 cm), 8 (36.13 cm), 10 (38.37 cm), 12 (40.49 cm), and 14 (42.46 cm) from top to bottom. In calibration, differences in fiber transmissions are corrected and instrumental broadening uses a helium calibration lamp, assuming $T_{\text{lamp}} = 0$. The instrumental function for each row of pixels is measured, and the spectra are fit as multiple Gaussian curves convolved with the measured instrumental function. Both raw data (black) and calibrated data (red) are shown after a dark frame subtraction to highlight photon counts. In this manuscript, units of Photons cm^{-2} sr^{-1} refer to the total number of photons collected at a given pixel.

III. EFFECTS DUE TO FINITE FLOW

The presence of plasma flows invalidates wavelength-by-wavelength inversion approaches,[9,11,12] such as Tanabe *et al.*[10] Instead, spectral moments are used to perform the tomographic inversions for emissivity, toroidal ion flow, and ion temperature.[13] The technique used to produce the results of Sec. V is a matrix inversion[14] that properly accounts for the effect of multi-component

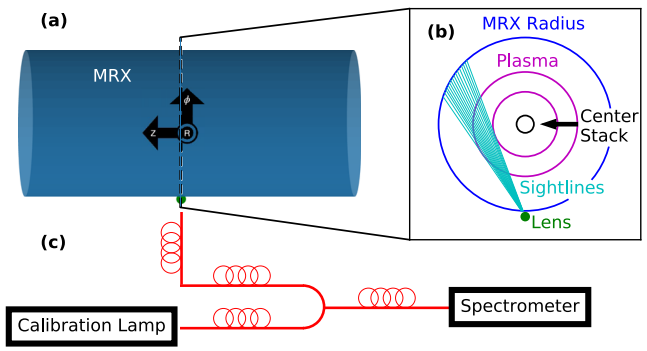

FIG. 1. Schematic of diagnostic measurements in MRX. (a) The experimental chamber of MRX with the reference coordinates. (b) Measurement geometry in the $R - \phi$ plane. (c) Path of the light from the chamber and calibration lamp into the spectrometer. Fiber optics are denoted in red.

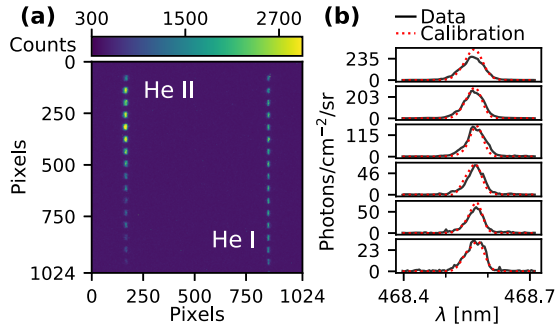

FIG. 2. (a) A raw image collected on the PI-MAX detector from discharge number 185006. Both He I [right-hand side of panel (a)] and He II [left-hand side of panel (a)] lines are visible. In this paper, only He II spectra are analyzed. (b) 6 of 16 measured spectra. From top to bottom, the spectra are from channels 4, 6, 8, 10, 12, and 14. The black lines show raw data, and the red lines show calibrated data.

flow across the measurement plane. This inversion assumes an axisymmetric plasma with emission modeled as

$$E(\lambda, R) = \frac{E_0(R)}{w(R)}\sqrt{\frac{4\ln 2}{\pi}}\exp\left[-4\ln 2\frac{(\lambda-\lambda_0-\frac{\lambda_0}{c}|\hat{s}_i\cdot\vec{v}(R)|)^2}{w^2(R)}\right], \quad (1)$$

where R is the radius, λ is the wavelength, E_0 is the scalar emissivity of the plasma, $2w$ is the full width at half maximum (FWHM) of the spectra due to thermal broadening, λ_0 is the rest wavelength of the measured emission, $\hat{s}_i$ is the unit vector in the direction of sightline, i, $\vec{v}$ is the local flow, and c is the speed of light.

Moments of the measured spectra are calculated and then quantized to zones of constant E_0, $\vec{v}$, and T_i between tangency radii.[11,14,15] These quantized moments in conjunction with length matrices representing the distance of a sightline between two constant zones of emission have been used to recover emissivity[15] and the toroidal component of velocity.[11] To properly solve for T_i, it is necessary to consider the geometry of plasma flow in the measurement plane for a diagnostic.

In MRX, the flow in the measurement plane of diagnostic sightlines contains components in the radial and toroidal directions. As pointed out by Bell,[14] only the toroidal flow component, v_ϕ, contributes to the Doppler shift of measured spectra; however, both components of the flow contribute to spectral broadening.[9,11,12] To invert for T_i, it is therefore necessary to supplement the results for E and v_ϕ with additional information about the projection $\vec{v}$ along all paths not perpendicular to $\hat{s}_i$. In the case of MRX, this requires measuring the radial flow component for the input to the inversion. For the results in Sec. V, this additional information comes from estimating $v_r \approx \frac{(\vec{E}\times\vec{B})_R}{B^2}$. The validity of this estimation will be addressed in future work.

With the complete set of projections of $\vec{v}$ along $\hat{s}_i$, the second moment of the measured spectra can be used to solve for T_i,

$$\delta\lambda^2(x_i) = \int_{-\infty}^{\infty} B_i(\lambda, x_i)(\lambda-\lambda_0)^2 d\lambda$$
$$= 2\int_R^{R_{edge}} \frac{E_0(R)RdR}{\sqrt{R^2-x_i^2}}\left[\frac{w^2(R)}{8\ln(2)} + \left(\frac{\lambda_0}{c}\right)^2 |\hat{s}_i\cdot\vec{v}(R)|^2\right], \quad (2)$$

where B_i is the brightness of viewing chord i. By first solving for emissivity and toroidal velocity, Eq. (2) is reduced to two unknowns: $w(R)$ and the radial component of $\vec{v}$. By assuming $\hat{s}_i = s_R\hat{\mathbf{R}} + s_\phi\hat{\phi} + 0\hat{\mathbf{Z}}$, we can explicitly describe the inner product of $\hat{s}_i$ and $\vec{v}$ as $\hat{s}_i\cdot\vec{v}(R) = \pm v_R\cos\theta^R_{i,j} + v_\phi\cos\theta^\phi_{i,j}$, where the transition from a continuum in R to quantized emission zones as described by Bell[11,15] is done implicitly. $\theta^R_{i,j}$ and $\theta^\phi_{i,j}$ are the angles between sightline i and the radial and toroidal components of velocity, respectively. The two angles are mathematical constructs and are not independent. The inversion for T_i can be carried out following the same prescription used for E_0 and v_ϕ from Bell,[11,15] with an additional matrix for the contribution of v_R to broadening.[14]

IV. NUMERICAL STUDY OF INVERSION

The inversion utilized in Sec. V is tested using Gaussian and hollow profiles in emissivity, E_0, and T_i. A parabolic profile for v_ϕ with a peak of −15 km/s is used and, except where varied as in Fig. 4(c), an identical profile is shown in Fig. 5(a) for v_R with a peak of ±15 km/s. The full width at half maximum (FWHM) of the Gaussian profiles was set to 5.5 cm, and the center of the profiles is located at R = 37.5 cm. The purpose of these numerical tests is to prove the integrity of the inversion technique outlined in Sec. III and used to produce results in Sec. V. The results are not informative regarding the expected uncertainties on MRX. Figures 3(a)–3(d) shows the four profile combinations used for E_0 and T_i as well as the success of a 35-chord inversion for each combination of profiles. Figure 3(e) shows the profile of v_ϕ used in the numerical tests with the inversion from case (a), corresponding to the Gaussian profiles in E_0 and T_i. The inversions of v_ϕ for the other three cases, corresponding to Figs. 3(b)–3(d), are equally successful and omitted for clarity in Fig. 3(e). For this simulation, a peak of 20 eV was used for T_i,

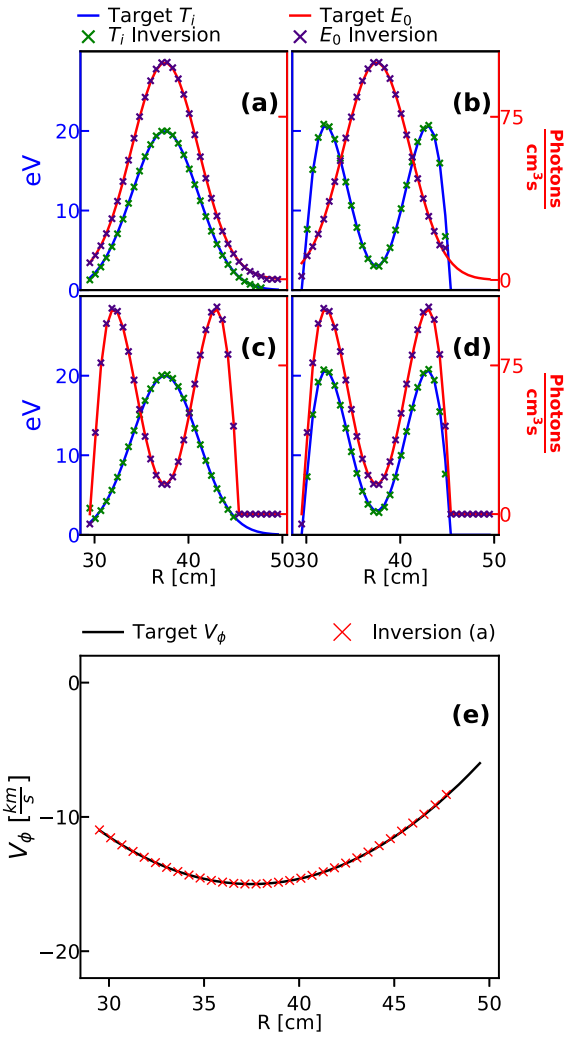

FIG. 3. Gaussian and Hollow profiles for E_0 (red) and T_i (blue) are shown in panels (a)–(d) along with 35-chord inversions of E_0 (purple) and T_i (green). The quadratic v_ϕ profile used in numerical tests is shown in panel (e), along with the inversion from the Gaussian/Gaussian combination of E_0 and T_i profiles corresponding to panel (a).

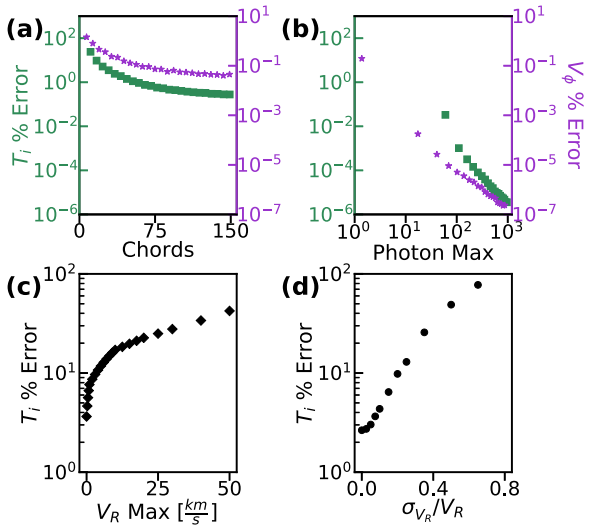

FIG. 4. Monte Carlo simulation (n = 10 000) of four different sources of error for Gaussian profiles in E_0 and T_i corresponding to Fig. 3(a). The total percentage error in T_i and V_ϕ inversions vs the number of measurement positions (a) is shown for a peak E_0 of 100, a peak v_R of 15 km/s, and a peak T_i of 20 eV. (b) Total inversion error of both quantities vs the peak photon count of E_0 for a 35-chord inversion. (c) Total error vs magnitude of v_R in a 35-chord inversion of T_i, assuming v_R = 0. (d) Total error of the T_i inversion vs the fractional standard deviation of v_R measurements for a 35-chord inversion.

E_0 was varied for the test presented in Fig. 4(b), and E_0 was set to 100 photons^{-1}/cm^{-3} for the other three tests in panels (a), (c), and (d).

To quantify the performance of the inversion algorithm used in Sec. V, four factors are investigated using 10 000 trials (n = 10 000) of a Monte Carlo simulation. The four parameters investigated are the number of viewing chords (measurement positions), photon counts, magnitude of v_R, and uncertainty in v_R measurements. The total error is calculated as a root mean squared (rms) percentage by summing over the deviation of the average of each point in the inversions of v_ϕ and T_i from the target profiles shown in Fig. 3 for all 10 000 trials. In each panel of Fig. 4, only the independent variable indicated in the caption is changed, while the other three parameters are held constant. The parameters used are 35 chords, photon max = 100, v_R^{Max} = 15 km/s, and σ_{v_R}/v_R = 0.1. The results of this numerical study provide confidence that the inversion technique used is computationally stable and convergent. It suggests that the technique can remain reliable even when the uncertainty of radial velocity measurements exceeds 20%.

V. EXPERIMENTAL RESULTS

Data were taken for more than 400 MRX discharges under a variety of field strengths, density, and temperature profiles. Sufficient light for a reliable inversion of 16 measurements was collected under multiple conditions and axial measurement locations. Measurements on most discharges were collected between t = 300 μs and t = 310 μs. At this early time, MRX is still in the "push" phase of reconnection,[3] where the two plasma toroids formed by the TF coils are being accelerated toward one another, to provide maximum light.

Figure 5(a) shows the v_R profile used as an input into the inversion, with a black dashed line indicating the zero velocity. This profile was calculated as $v_R = \frac{\vec{E}\times\vec{B}}{B^2}$, where measurements of $\vec{E}$ are derived from the measurements of $\vec{B}$, made with MRX magnetics probes.[16] Figure 5(b) shows the contributions to the Doppler broadening of measured spectra from T_i (orange), v_R (purple), and v_ϕ (red). The apparent temperature (blue) is the "temperature" of the measured spectra based on the width of the spectra. The contributions from other sources quantify the broadening of the spectra, in electron volts, from each of the flow components and the ion temperature. Figure 5(c) shows the v_ϕ (red) and T_i (blue) inversions for discharge No. 185006. Regions of plasma beyond R = 40.14 cm are too dim to provide physically meaningful data.

The error bars in Fig. 5 show one standard deviation calculated by propagating the inherent uncertainty of spectral measurement due to Poisson statistics across the full inversion. The linear nature of the inversion makes these calculations tractable. No systematic error is considered and is likely why the inner-most point, located at R = 28.6 cm, has negligible error. Additionally, the representations of temperature contribution from Fig. 5(b) appear to go negative near R = 30 cm due to an improper accounting of the regions outside $R = R_{max}$. Not measuring to the plasma edge causes the inversion to overestimate the outside regions and underestimate

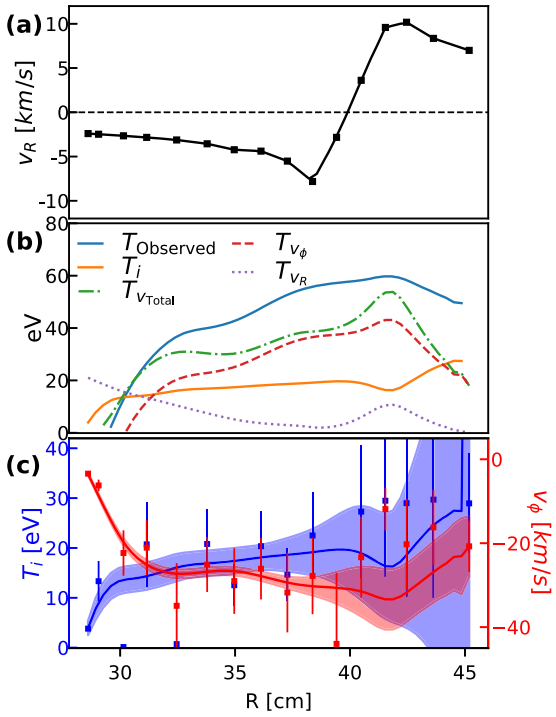

FIG. 5. (a) Radial velocity profile from MRX discharge No. 185006 in km/s with a horizontal line at v_R = 0. (b) Contributions to the apparent ion temperature from various sources. Notice non-negligible contribution from v_R, even at v_R^{peak} ~ 10 km/s. (c) Inversions of T_i (blue) and v_ϕ (red) with shaded error represented one standard deviation.

the inside regions. A full accounting of error sources, necessary for physics experiments, would include error in the alignment of collection optics, beam divergence, and a consideration of error in the instrumental temperature. These systematic sources of error are beyond the scope of this paper. The lines and shading region show an inversion on a smoothed and interpolated dataset. To perform the inversion, the moments of the measured spectra are smoothed using a smoothing spline,[14,17] weighted by the standard deviation of the moments (originating from Poisson statistics). The inversion is then performed on the smoothed moments and the results are shown in red for v_R and blue for T_i in Fig. 5(c). The shading of the splines represents the standard deviation of the smoothed data, which is calculated by running $n = 1000$ Monte Carlo simulations where the moments are varied randomly within their standard deviation each trial before a spline is fit and an inversion is performed. This method can be useful for systems with limited sightlines, as is the case here. The numerical performance of inverting smoothed data will be evaluated in future work, if necessary. It is likely that with more sightlines on MRX, a smoothing spline will not provide a meaningful benefit in the inversion process.

VI. CONCLUSION

A new implementation of tomographic ion temperature measurements is presented here. The hardware setup outlined is robust and economical. Proper consideration of multi-component flow in the measurement plane of a two-dimensional plasma is presented, and it is shown that a commercially available lens along with mounting hardware and a linear fiber array passed into a spectrometer is sufficient to get reliable inversion of toroidal flow and ion temperature in MRX, provided an estimate or measurement of v_R profiles. To the authors' knowledge, this marks the first implementation of a tomographic ion Doppler diagnostic inverting low (~ 10 eV) ion temperatures in the presence of two-component in-plane flows by properly treating the effects of radial flow.

Numerical calculations confirm the fidelity of the matrix inversion method and an investigation of the effects of radial velocity on the inversion show that magnitudes of radial velocity ~ 10 km/s can lead to errors in the inversion of ion temperature of $\approx 15\%$ if not properly treated. It is also shown that uncertainties in radial velocity measurements of 20% lead to T_i inversion errors of $\approx 10\%$.

This work lays the groundwork for a full scale diagnostic of this design using 80 measurement chords and a higher throughput spectrometer (f/1.8). This diagnostic is being installed on MRX and new data will soon follow.

ACKNOWLEDGMENTS

The authors thank Dr. R. E. Bell for consultation on both hardware design and implementation of this novel tomographic inversion and P. Sloboda for his technical assistance. This research was supported by the Department of Energy (Contract No. DE-SC0019049).

DATA AVAILABILITY

The data that support the findings of this study are available from the corresponding author upon reasonable request.

REFERENCES

[1] M. Yamada, R. Kulsrud, and H. Ji, Rev. Mod. Phys. **82**, 603 (2010).
[2] M. Yamada, J. Yoo, J. Jara-Almonte *et al.*, Nat. Commun. **5**, 4774 (2014).
[3] M. Yamada *et al.*, Phys. Plasmas **4**, 1936 (1997).
[4] G. Fiksel, D. J. Den Hartog, and P. W. Fontana, Rev. Sci. Instrum. **69**, 2024 (1998).
[5] K.-S. Chung, Plasma Sources Sci. Technol. **21**, 063001 (2012).
[6] H. Ji *et al.*, J. Am. Astron. Soc. **1**, 104–105 (2015).
[7] A. M. Cormack, J. Appl. Phys. **34**, 2722 (1963).
[8] R. S. Granetz and P. Smeulders, Nucl. Fusion **28**, 457 (1988).
[9] N. P. Efremov, N. P. Poluektov, and V. N. Kharchenko, J. Quant. Spectrosc. Radiat. Transfer **53**, 723 (1995).
[10] H. Tanabe, A. Kuwahata, H. Oka, M. Annoura, H. Koike, K. Nishida, S. You, Y. Narushima, A. Balandin, M. Inomoto, and Y. Ono, Nucl. Fusion **53**, 093027 (2013).
[11] R. E. Bell, Rev. Sci. Instrum. **68**, 1273 (1997).
[12] N. P. Poluektov and N. P. Efremov, J. Phys. D: Appl. Phys. **31**, 988 (1998).
[13] J. Howard, Plasma Phys. Controlled Fusion **38**, 489 (1996).
[14] R. E. Bell, Plasma Phys. Controlled Fusion **63**, 045023 (2021).
[15] R. E. Bell, Rev. Sci. Instrum. **66**, 558 (1995).
[16] J. Yoo, M. Yamada, H. Ji, J. Jara-Almonte, and C. E. Myers, Phys. Plasmas **21**, 055706 (2014).
[17] C. H. Reinsch, Numerische Math. **10**, 177 (1967).